



Shakedown analysis of porous materials via mixed meshless methods

Carlos C. de La Plata Ruiz¹ · Jose Luis Silveira²

Received: 4 February 2020 / Accepted: 4 May 2020 / Published online: 15 May 2020
© The Brazilian Society of Mechanical Sciences and Engineering 2020

Abstract

In this paper, the elastic shakedown analysis of porous materials is performed by means of meshless methods using mixed approximations. Based on a mixed variational principle for shakedown analysis and using a yield function for porous materials, two meshless methods are adapted to perform mixed approximations of the stress and velocity fields for the solution of the discrete shakedown problem. These two new methods are named mixed moving least squares method and mixed Shepard's method and are used to solve some numerical examples. The numerical results obtained showed a good agreement with available analytical solutions and published results by the finite element method. The proposed mixed methods can be applied in the analysis of structural and machine parts made of porous materials and subjected to variable loads.

Keywords Plasticity · Shakedown analysis · Porous material · Yield function · Meshless method

1 Introduction

Shakedown analysis enables to find the safe condition of operation for structures under variable loads and has been used in the design of several applications, such as pressure vessels and components for aerospace industry. The first studies on this subject started in the 1920s. Weichert and Ponter [33] presented a comprehensive historical introduction on shakedown theory and pointed out that the first contribution to an embryonic idea of shakedown was due to Gruning in the mid-1920s. Bleich and Melan's later contributions gave rise to the lower-bound shakedown theorem [22], and subsequently Koiter established the upper-bound theorem [16] in the context of ideal plasticity.

Over the years, shakedown theory has been refined and expanded to solve more complex problems with the aid of numerical methods. In particular, the finite element method

(FEM) is one of the most used techniques. Belytschko [2] was the first to apply the FEM for the solution of a shakedown problem. He obtained the numerical solution for the shakedown of a plate with a circular hole in a state of plane stress, which became a benchmark for this subject. However, despite its successful application, the finite element method is not the only method used for the numerical shakedown solution. Based on the meshless local Petrov–Galerkin (MLPG) method, Chen et al. [7] presented a solution procedure for the lower-bound shakedown analysis and Ruiz and Silveira [27] proposed a generalization of the moving least squares method [3] to solve shakedown problems using mixed approximations. Along with the methods for spatial discretization, several procedures and algorithms have been proposed to solve the shakedown problems numerically. Mathematical programming has been widely used in numerical shakedown analysis. The pioneering works in this field are due to Maier [19, 20], who introduced linear programming in the limit and shakedown analysis problems. Several interior point methods with different iteration schemes have been successfully proposed [11, 23, 38]. Makrodimitropoulos [21] and Krabbenhøft et al. [17] applied conic programming to solve shakedown problems. Apart from mathematical programming methods, other types of approaches have been used successfully. Chen and Ponter [6] developed the linear matching method (LMM), which performs a sequence of linear solutions with spatially varying moduli to match the linear behavior to the nonlinear plastic behavior. More recently, Peng et al. [25, 26] developed

Technical Editor: João Marciano Laredo dos Reis.

✉ Jose Luis Silveira
jluis@mecanica.ufrj.br

Carlos C. de La Plata Ruiz
delaplataruiz@uol.com.br

¹ Department of Mechanical Engineering, Universidade do Estado do Rio de Janeiro, Rio de Janeiro, Brazil

² Department of Mechanical Engineering, Universidade Federal do Rio de Janeiro, Rio de Janeiro, Brazil

a numerical procedure called stress compensation method (SCM) suitable for shakedown analysis of realistic engineering structures subjected to variable loads.

Most numerical solutions for shakedown analysis have been applied to solve problems involving dense materials. Recently, the numerical solution for the shakedown of porous materials has received a growing attention. Zhang et al. [35] considered a hollow sphere model to obtain shakedown solutions of porous materials under cyclic loads. Using variational principles and the finite element method, Ruiz and Silveira [28] presented numerical solutions for the shakedown analysis of porous materials.

The constitutive behavior of the porous materials should be described by a suitable yield function for the shakedown analysis. Several authors proposed yield functions for this type of material [8, 9, 12, 14, 24, 28, 30].

In this paper, the mixed moving least squares method proposed by Ruiz and Silveira [27] is applied to the shakedown analysis of porous materials. In the next section, a yield function for porous material is presented [28]. This yield function is used in the numerical solution of the mixed variational principle for shakedown analysis of porous material presented in Sect. 3. Two meshless methods are used to solve the shakedown problem, namely the mixed moving least squares method developed in Sect. 4 and the mixed Shepard’s method presented in Sect. 5. Finally, some numerical examples are solved in Sect. 6.

2 A yield function for porous material

The yield function used in the shakedown analysis of porous material presented in this paper is based on a previous proposal [8, 28], as shown in the following:

$$f(T, R) = A(R)J_2(T) + B(R)I_1^2(T) - \delta(R)Y_0^2 \leq 0 \tag{1}$$

where R is the relative density of the material; T is the stress tensor; Y_0 is the yield limit of the base material; J_2 is the second invariant of the stress deviator tensor; I_1 is the first invariant of the stress tensor; and A and B are given by the following expressions:

$$A(R) = 2 + R^n \tag{2}$$

$$B(R) = \frac{(1 - R^n)}{3} \tag{3}$$

In this paper, n and $\delta(R)$ are given by the expressions proposed by Alves et al. [1]:

$$n = 4.15R_i - 1.23 \tag{4}$$

$$\delta(R) = \frac{0.343R_i^{2.988} R}{0.343R_i^{2.988} + (1 - R)} \tag{5}$$

where R_i is the initial relative density of the porous material and the relative density R is given by the expression proposed by Heckel [15]:

$$R = 1 - e^{-[k p + \ln(\frac{1}{1-R_i})]} \tag{6}$$

where p is a compressive hydrostatic pressure acting in the material and k is given by Heckel [15]:

$$k \cong \frac{1}{3Y_0} \tag{7}$$

The compressive hydrostatic pressure p can be computed by the following expression, from the trace of the residual stress tensor T^r obtained by the shakedown analysis [28]:

$$p = -\frac{1}{3}\text{tr}(T^r) \tag{8}$$

Therefore, from Eq. (8), the expression (6) proposed by Heckel [15] becomes a function of the residual stress T^r . Consequently, Eqs. (2), (3) and (5) become functions of the residual stress: $A(T^r)$, $B(T^r)$ and $\delta(T^r)$.

In the solution of the shakedown problem, as shown in Sect. 3, the stress T is given by the contribution of a residual and an elastic part, represented by T^e and T^r , respectively:

$$T = T^e + T^r \tag{9}$$

In view of Eqs. (6), (8) and (9), the yield function (1) can be rewritten as:

$$f(T^e, T^r) = A(T^r)J_2(T^e + T^r) + B(T^r)I_1^2(T^e + T^r) - \delta(T^r)Y_0^2 \leq 0 \tag{10}$$

It’s worth mentioning that the previous expression was developed for a stress state at a point. This yield condition can be considered as a modified von Mises yield function, which includes the influence of the hydrostatic stress. For each point in the body, given a hydrostatic stress value, the yield function is represented by the graph of an ellipsis, which limits a convex set in the stress space [18]. The convexity of the yield function allows the assumption of associate plasticity, which is used in the solution of the shakedown analysis [28].

In the next section, a version of the yield function (10) in terms of stress fields will be used, as given by:

$$f(\mathbf{T}^e + \mathbf{T}^r) = A(\mathbf{T}^r)J_2(\mathbf{T}^e + \mathbf{T}^r) + B(\mathbf{T}^r)I_1^2(\mathbf{T}^e + \mathbf{T}^r) - \delta(\mathbf{T}^r)Y_0^2 \leq 0 \tag{11}$$

where \mathbf{T}^e represents the elastic stress field and \mathbf{T}^r is the residual stress field in the porous body.

3 Shakedown analysis of porous materials

3.1 Notation for kinematics and equilibrium

In this paper, V represents the space of velocity fields \mathbf{v} and W is the space of strain rate fields $\dot{\epsilon}$. A kinematically compatible velocity field $\mathbf{v} \in V$ is related to a strain rate field $\dot{\epsilon} \in W$ by the following relation:

$$\dot{\epsilon} = D\mathbf{v} \quad \mathbf{v} \in V \quad \text{and} \quad \dot{\epsilon} \in W \tag{12}$$

The operator D represents the linear deformation operator and is defined by:

$$D = \frac{1}{2}(\nabla \cdot + \nabla^T \cdot) \tag{13}$$

Let B be the region in \mathbb{R}^3 occupied by a body subjected to surface tractions τ specified in the portion Γ_τ of the boundary of B . The space of stress fields \mathbf{T} is represented by W' ; moreover, a stress field $\mathbf{T} \in W'$, in equilibrium with the external loads, satisfies the following relation:

$$\int_B \mathbf{T} \cdot D\mathbf{v} \, dB = \int_B \mathbf{b} \cdot \mathbf{v} \, dB + \int_{\Gamma_\tau} \tau \cdot \mathbf{v} \, d\Gamma_\tau \quad \forall \mathbf{v} \in V \tag{14}$$

where \mathbf{b} is the body force field.

In a more compact form, Eq. (14) can be written as:

$$\langle \mathbf{T}, D\mathbf{v} \rangle = \langle F, \mathbf{v} \rangle \quad \forall \mathbf{v} \in V \tag{15}$$

where the internal and external powers are expressed, respectively, by:

$$\langle \mathbf{T}, D\mathbf{v} \rangle = \int_B \mathbf{T} \cdot D\mathbf{v} \, dB \tag{16}$$

$$\langle F, \mathbf{v} \rangle = \int_B \mathbf{b} \cdot \mathbf{v} \, dB + \int_{\Gamma_\tau} \tau \cdot \mathbf{v} \, d\Gamma_\tau \tag{17}$$

A self-equilibrated stress field \mathbf{T}^r is defined as the stress field that equilibrates a null external load; therefore, it can be described by the following equation:

$$\langle \mathbf{T}^r, D\mathbf{v} \rangle = 0 \quad \forall \mathbf{v} \in V \tag{18}$$

In the next section, the yield function for porous materials presented in Sect. 2 will be used in the development of a mixed variational principle for the shakedown analysis of porous materials.

3.2 A mixed variational principle for shakedown of porous material

Based on previous works [28, 31, 36, 37], a mixed variational principle for the shakedown analysis of porous materials is presented in this section. This mixed principle allows to obtain the maximum amplification factor ω for a polyhedral domain of load variation, such that the material shakes down elastically under any load variation contained within the polyhedral domain.

For α mechanically independent loads acting on a body, the load domain is composed by a convex polyhedron with m vertices, where $m = 2^\alpha$ and the following mixed variational principle can be written:

$$\omega = \sup_{\omega^*, \mathbf{T}^r} \inf_{\mathbf{v}} [\omega^* + \langle \mathbf{T}^r, D\mathbf{v} \rangle] \Big| f(\omega^* \mathbf{T}^{e\alpha} + \mathbf{T}^r) \leq 0 \quad \alpha = 1 \dots m \tag{19}$$

where $\mathbf{T}^{e\alpha}$ represents the unlimited elastic stress field for each vertex α , \mathbf{T}^r is a residual stress field, D is the linear deformation operator, and \mathbf{v} is a kinematically compatible velocity field.

A discrete form for the variational principle (19) can be written as follows:

$$\omega = \max_{\omega^*, \hat{\mathbf{T}}^r} \min_{\hat{\mathbf{v}}} \left[\omega^* + \int_B \hat{\mathbf{T}}^r \cdot D\hat{\mathbf{v}} \, dB \right] \Big| f(\omega^* \hat{\mathbf{T}}^{e\alpha} + \hat{\mathbf{T}}^r) \leq 0 \quad \alpha = 1 \dots m \tag{20}$$

where $\hat{\mathbf{T}}^r$ and $\hat{\mathbf{v}}$ are approximations for the residual stress and velocity fields, respectively, and $\hat{\mathbf{T}}^{e\alpha}$ is an approximated unlimitedly elastic stress field, which can be obtained by a numerical or an analytical solution.

The velocity and residual stress fields can be approximated as follows:

$$\hat{\mathbf{v}} = \Phi \mathbf{v} \tag{21}$$

$$\hat{\mathbf{T}}^r = \Theta T \tag{22}$$

where Φ represents a matrix of velocity shape functions, Θ is a matrix of stress shape functions, and \mathbf{v} and T are the vectors with the nodal values of velocities and residual stresses, respectively.

Substituting Eqs. (21) and (22) into (20), the following mixed discrete principle is obtained:

$$\omega = \max_{\omega^*, T} \min_{\mathbf{v}} [\omega^* + T \cdot \mathbf{B}\mathbf{v}] \Big| f(\omega^* T^{e\alpha} + T) \leq 0 \tag{23}$$

$$\alpha = 1 \dots m$$

where $T^{e\alpha}$ represents a vector whose components correspond to the values of unlimitedly elastic stress field at the nodal or base points and \mathbf{B} is a matrix given by the following:

$$\mathbf{B} = \int_B \boldsymbol{\Theta}^T D\boldsymbol{\Phi} dB \tag{24}$$

Among the several possible ways to build the matrix \mathbf{B} , two forms are presented in this paper: the first, named mixed moving least squares method, is developed in Sect. 4; and the second, named mixed Shepard’s method, is presented in Sect. 5.

4 Mixed moving least squares method

In this section, a generalization of the moving least squares (MLS) method proposed by Belytschko et al. [4] is presented. Based on Belytschko’s proposal, Ruiz and Silveira [27] generalized the moving least squares method through a mixed approximation for the velocity and stress fields.

For a shakedown numerical solution by the mixed moving least squares method (MixMLS), the approximate velocity and stress fields are given, respectively, by the relations (21) and (22). In this method, $\boldsymbol{\Phi}$ represents the matrix of velocity shape functions $\phi_i(\mathbf{x})$ given by Eq. (25) and $\boldsymbol{\Theta}$ is the matrix of stress shape functions $\theta_i(\mathbf{x})$ given by Eq. (26), as follows:

$$\phi_i(\mathbf{x}) = w(d_i) \mathbf{p}(\mathbf{x}) \cdot \mathbf{A}^{-1}(\mathbf{x}) \mathbf{p}(\mathbf{x}_i) \tag{25}$$

$$\theta_i(\mathbf{x}) = w(d_i) \mathbf{q}(\mathbf{x}) \cdot \mathbf{C}^{-1}(\mathbf{x}) \mathbf{q}(\mathbf{x}_i) \tag{26}$$

where w is a radial basis function.

Many radial basis functions are possible to solve shakedown problems. Some of these functions have been tested (not shown in the paper), and the two of them, which showed the best results, are presented:

- the exponential radial basis function [3], given by:

$$w(d_i) = \frac{e^{-(d_i/c)^2} - e^{-(1/c)^2}}{1 - e^{-(1/c)^2}} \tag{27}$$

- and the expression proposed by Wu [34]:

$$w(d_i) = (1 - d_i)^7 (5 + 35d_i + 101d_i^2 + 147d_i^3 + 101d_i^4 + 35d_i^5 + 5d_i^6) \tag{28}$$

where c in Eq. (27) is a characteristic length related to the distance between the nodal points.

The distance d_i used in the previous expressions is defined by:

$$d_i = \frac{1}{r} \|\mathbf{x} - \mathbf{x}_i\| \tag{29}$$

where $\|\mathbf{x} - \mathbf{x}_i\|$ is the distance between the point \mathbf{x} and the base point \mathbf{x}_i and r represents the support radius of the radial basis function. According to Guedes [13], for equally spaced

nodal points, the value of r can be taken between 2 and 6 times the nodal distance.

The vector \mathbf{p} in Eq. (25) and the vector \mathbf{q} in Eq. (26) are composed by monomial basis functions components. In the present paper, for a two-dimensional space analysis, \mathbf{p} and \mathbf{q} are given by the following vectors:

$$\mathbf{p}(\mathbf{x}) = \mathbf{p}(x, y) = [1 \quad x \quad y \quad x^2 \quad xy \quad y^2]^T \tag{30}$$

$$\mathbf{q}(\mathbf{x}) = \mathbf{q}(x, y) = [1 \quad x \quad y]^T \tag{31}$$

where x and y refers to the Cartesian coordinates of any point \mathbf{x} in the two-dimensional space.

The matrices \mathbf{A} in Eq. (25) and \mathbf{C} in Eq. (26) are given, respectively, by the following relations:

$$\mathbf{A} = \mathbf{P}^T \mathbf{W} \mathbf{P} \tag{32}$$

$$\mathbf{C} = \mathbf{Q}^T \mathbf{W} \mathbf{Q} \tag{33}$$

where, for n base points, \mathbf{W} is a diagonal matrix $n \times n$ given by:

$$\mathbf{W} = \text{diag}[w(d_i)] \tag{34}$$

The matrices \mathbf{P} and \mathbf{Q} are, respectively, given by:

$$\mathbf{P} = [\mathbf{p}(\mathbf{x}_1) \quad \mathbf{p}(\mathbf{x}_2) \quad \mathbf{p}(\mathbf{x}_3) \quad \dots \quad \mathbf{p}(\mathbf{x}_n)]^T \tag{35}$$

$$\mathbf{Q} = [\mathbf{q}(\mathbf{x}_1) \quad \mathbf{q}(\mathbf{x}_2) \quad \mathbf{q}(\mathbf{x}_3) \quad \dots \quad \mathbf{q}(\mathbf{x}_n)]^T \tag{36}$$

According to expression (24), the matrix \mathbf{B} in the mixed variational principle (23) is obtained by the integration of the product of the stress approximation matrix $\boldsymbol{\Theta}$ and the matrix $D\boldsymbol{\Phi}$ of the derivatives of the velocity shape functions. Therefore, the derivatives of the velocity shape functions are required.

For an analysis in the plane, the matrix $\boldsymbol{\Theta}$ and the matrix $D\boldsymbol{\Phi}(x, y)$ are given by the following:

$$\boldsymbol{\Theta} = \begin{bmatrix} \theta_1 & 0 & 0 & \theta_2 & 0 & 0 & \dots & \theta_{n-1} & 0 & 0 & \theta_n & 0 & 0 \\ 0 & \theta_1 & 0 & 0 & \theta_2 & 0 & \dots & 0 & \theta_{n-1} & 0 & 0 & \theta_n & 0 \\ 0 & 0 & \theta_1 & 0 & 0 & \theta_2 & \dots & 0 & 0 & \theta_{n-1} & 0 & 0 & \theta_n \end{bmatrix} \tag{37}$$

$$D\boldsymbol{\Phi} = \begin{bmatrix} \phi_{1,x} & 0 & \phi_{2,x} & 0 & \dots & \phi_{n-1,x} & 0 & \phi_{n,x} & 0 \\ 0 & \phi_{1,y} & 0 & \phi_{2,y} & \dots & 0 & \phi_{n-1,y} & 0 & \phi_{n,y} \\ \phi_{1,y} & \phi_{1,x} & \phi_{2,y} & \phi_{2,x} & \dots & \phi_{n-1,y} & \phi_{n-1,x} & \phi_{n,y} & \phi_{n,x} \end{bmatrix} \tag{38}$$

In the previous matrix, $\phi_{i,x}$ and $\phi_{i,y}$ represent the partial derivatives of the velocity shape functions $\phi_i(\mathbf{x})$ with respect to x and y , respectively, and are given by:

$$\begin{aligned} \phi_{i,x} &= \mathbf{L}_{,x}\mathbf{E} + \mathbf{L}\mathbf{E}_{,x} \quad \text{and} \\ \phi_{i,y} &= \mathbf{L}_{,y}\mathbf{E} + \mathbf{L}\mathbf{E}_{,y} \end{aligned} \tag{39}$$

where \mathbf{E} and \mathbf{L} are given by the following expressions [10]:

$$\mathbf{E} = w(d_i)\mathbf{p}(\mathbf{x}_i) \tag{40}$$

$$\mathbf{L} = \mathbf{p}^T(\mathbf{x})\mathbf{A}^{-1} \tag{41}$$

and the corresponding derivatives of \mathbf{E} and \mathbf{L} are given by:

$$\begin{aligned} \mathbf{E}_{,x} &= w(d_{i,x})\mathbf{p}(\mathbf{x}_i) \quad \text{and} \\ \mathbf{E}_{,y} &= w(d_{i,y})\mathbf{p}(\mathbf{x}_i) \end{aligned} \tag{42}$$

$$\mathbf{L}_{,x} = \mathbf{p}^T(\mathbf{x})_{,x}\mathbf{A}^{-1} + \mathbf{p}^T(\mathbf{x})\mathbf{A}_{,x}^{-1} \tag{43}$$

$$\mathbf{L}_{,y} = \mathbf{p}^T(\mathbf{x})_{,y}\mathbf{A}^{-1} + \mathbf{p}^T(\mathbf{x})\mathbf{A}_{,y}^{-1} \tag{44}$$

where

$$\mathbf{A}_{,x}^{-1} = -\mathbf{A}^{-1}[\mathbf{P}^T\mathbf{W}_{,x}\mathbf{P}]\mathbf{A}^{-1} \tag{45}$$

$$\mathbf{A}_{,y}^{-1} = -\mathbf{A}^{-1}[\mathbf{P}^T\mathbf{W}_{,y}\mathbf{P}]\mathbf{A}^{-1} \tag{46}$$

In expressions (45) and (46), $\mathbf{W}_{,x}$ and $\mathbf{W}_{,y}$ are diagonal matrices of the derivatives of the weight function w , Eqs. (27) and (28), with respect to x and y , respectively:

$$w_{,x} = w_{,d_i}d_{i,x} \quad \text{and} \quad w_{,y} = w_{,d_i}d_{i,y} \tag{47}$$

where

$$d_{i,x} = \frac{x - x_i}{r d_i} \quad \text{and} \quad d_{i,y} = \frac{y - y_i}{r d_i} \tag{48}$$

and $w_{,d_i}$ is the derivative of the weight function with respect to d_i .

Upon obtaining the matrix $D\Phi$, the numerical integration of the product $\Theta^T D\Phi$ yields the matrix \mathbf{B} . In Sect. 6, some numerical examples are presented for the moving least squares method with mixed approximation.

There is a minimum number of nodes for the MixMLS method to converge, which depends on the number of monomials in the chosen polynomials. In this paper, the minimum number of nodes is nine, because a linear polynomial basis function is used to approximate the stress field and a quadratic polynomial basis function is used to approximate the velocity field.

5 Mixed Shepard’s method

The method proposed by Shepard [29] can be considered as a particular case of the moving least squares method. In this section, a generalization of the Shepard’s method is presented, through a mixed approximation for the stress and velocity fields. In the mixed Shepard’s (MixS) method, the polynomial bases $\mathbf{p}(\mathbf{x})$, Eq. (30), and $\mathbf{q}(\mathbf{x})$, Eq. (31), are composed of a single element.

$$\mathbf{p} = \mathbf{q} = [1] \tag{49}$$

Consequently, the matrices $\mathbf{A}(\mathbf{x})$, Eq. (32), and $\mathbf{C}(\mathbf{x})$, Eq. (33), become a scalar given by:

$$\mathbf{A}(\mathbf{x}) = \mathbf{C}(\mathbf{x}) = \sum_{i=1}^n w(d_i) \tag{50}$$

and the shape functions $\phi_i(\mathbf{x})$, Eq. (25), and $\theta_i(\mathbf{x})$, Eq. (26), can be obtained by the following expression:

$$\phi_i(\mathbf{x}) = \theta_i(\mathbf{x}) = \frac{w(d_i)}{\sum_{j=1}^n w(d_j)} \tag{51}$$

In the next section, some numerical examples for the shakedown analysis of porous materials are presented using the mixed moving least squares method and the mixed Shepard’s method. The simulations are performed by applying an interior point algorithm [38], which performs a Newton iteration to solve the nonlinear constrained optimization problem given by Eq. (23).

6 Numerical examples

In this section, the numerical analysis of the shakedown of porous material is presented. The yield function described by Eq. (11) is used, together with the values of the Young’s modulus E , the Poisson’s ratio ν , and the thermal expansion coefficient c given by the following expressions:

$$E = E_0 R^{n_E} \tag{52}$$

$$\nu = \nu_0 R^{n_\nu} \tag{53}$$

$$c = c_0 R^{n_c} \tag{54}$$

where E_0 , ν_0 , and c_0 are the corresponding material properties for the base material, i.e., material properties for a relative density equal 1.0 and the exponents n_E , n_ν , and n_c are arbitrarily taken as unity.

In the following examples, when a tensile residual stress state occurs, it is assumed that the relative density does not present any variation [28].

6.1 A rod of porous material subjected to axial load and temperature variation

In this section, the shakedown analysis of a rod made of porous material is presented. The rod is subjected to an axial load and a non uniform field of temperature variation. The axial load F is applied at an intermediate point along the rod's length L as shown in Fig. 1. The temperature θ and the axial load F can vary independently. The rod is composed by two separate regions, named α and β . The temperature field is restricted to the region α of the rod. The rod ends are clamped, and the regions α and β have lengths aL and bL , respectively. The cross section of the rod is equal to A and the material has a initial relative density R_i .

The following non-dimensional parameters for the load and temperature are used, respectively:

$$p = \frac{F}{2AY_0} \tag{55}$$

$$q = \frac{Ec\theta}{Y_0} \tag{56}$$

where Y_0 represents the yield stress for the base material, E represents the Young's modulus, and c is the thermal expansion coefficient, given by Eqs. (52) and (54), respectively.

The limits for the variation of the non-dimensional parameters p and q are given by:

$$0 \leq p \leq \bar{p} \quad 0 \leq q \leq \bar{q} \tag{57}$$

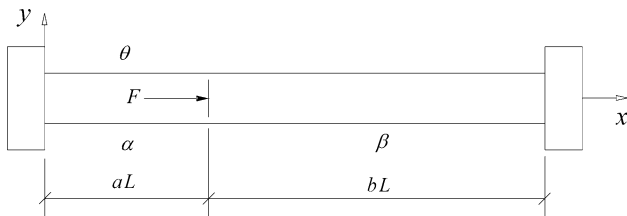
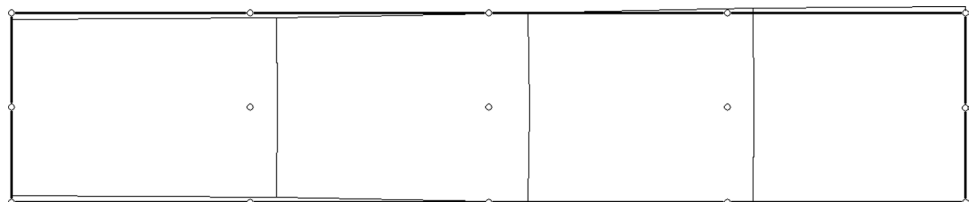


Fig. 1 Clamped rod of porous material subjected to axial load and temperature variation

Fig. 2 Nodes distribution and deformation aspect for the rod



where \bar{p} and \bar{q} are the maximum values for p and q , respectively. Therefore, the limits for the variation of p and q define a quadrilateral domain for the load variation.

Following Silveira and Zouain [31], the elastic stresses for the regions α and β are given by:

$$T_\alpha^1 = 2b\bar{p}Y_0 \quad T_\beta^1 = -2a\bar{p}Y_0 \tag{58}$$

$$T_\alpha^2 = (2b\bar{p} - a\bar{q})Y_0 \quad T_\beta^2 = (-2a\bar{p} - a\bar{q})Y_0 \tag{59}$$

$$T_\alpha^3 = -a\bar{q}Y_0 \quad T_\beta^3 = -a\bar{q}Y_0 \tag{60}$$

$$T_\alpha^4 = 0 \quad T_\beta^4 = 0 \tag{61}$$

where the indices 1, 2, 3, and 4 correspond to each vertex of the quadrilateral domain for the load variation.

For $b \geq a$, the analytical solution for the amplification factor is given by [31]:

$$\omega_a = \frac{2}{2\bar{p} + a\bar{q}} \tag{62}$$

Figure 2 shows the 15 nodal points distributed along the rod and the deformation aspect obtained from the solution by the mixed moving least squares (MixMLS) method for a rod with a relative density equal 1.0. A quadratic polynomial basis function was used to approximate the velocity field and a linear polynomial basis function to approximate the stress field. The radial basis function (28) proposed by Wu [34] was employed with a support radius equal to two and a half times the nodal distance in the rod axis direction.

Table 1 compares the numerical results obtained for the mixed moving least squares (MixMLS) method and the mixed Shepard's (MixS) method with the numerical results obtained by the finite element method (FEM) [28]. The finite element mesh used to solve this example has 160 triangular elements, with 369 nodes for velocities and 105 nodes for stresses. The element used is a mixed triangular finite element which is composed by six nodes of velocities and three nodes of stresses and is described in detail in Borges et al. [5] and Zouain et al. [39].

The numerical results are obtained for the particular case of a rod with $L = 1$ m, $A = 0.01$ m², maximum axial load $\bar{F} = 1$ MN, maximum temperature $\bar{\theta} = 250$ °C,

Table 1 Numerical comparison for the mixed moving least squares, mixed Shepard’s, and finite element method for the rod made of porous material

	R_i	ω	$\omega\bar{p}$	$\omega\bar{q}$	$T_{x_{avg}}^r$ (MPa)	Ampl. T_x^r (MPa)	R_{avg}	Ampl. R
MixMLS	0.7	2.993	0.1871	1.283	179.6	10.9	0.7074	1.51×10^{-3}
MixS	0.7	2.605	0.1628	1.117	147.3	131.2	0.7060	6.05×10^{-3}
FEM	0.7	3.006	0.1878	1.289	180.6	41.8	0.7074	3.02×10^{-3}
MixMLS	0.8	3.499	0.2187	1.960	284.3	41.2	0.8077	3.40×10^{-3}
MixS	0.8	2.986	0.1866	1.672	229.5	259.3	0.8063	8.68×10^{-3}
FEM	0.8	3.517	0.2198	1.970	286.1	47.6	0.8078	2.38×10^{-3}
MixMLS	0.9	3.912	0.2445	2.772	409.3	9.2	0.9055	3.80×10^{-3}
MixS	0.9	3.283	0.2052	2.327	325.1	384.3	0.9044	6.35×10^{-4}
FEM	0.9	3.936	0.2460	2.790	412.5	52.2	0.9056	1.41×10^{-3}
MixMLS	1.0	4.178	0.2611	3.656	542.3	179.6	1.0000	6.58×10^{-8}
MixS	1.0	3.461	0.2163	3.028	425.0	519.2	1.0000	8.51×10^{-8}
FEM	1.0	4.211	0.2632	3.684	547.4	59.9	1.0000	1.66×10^{-8}

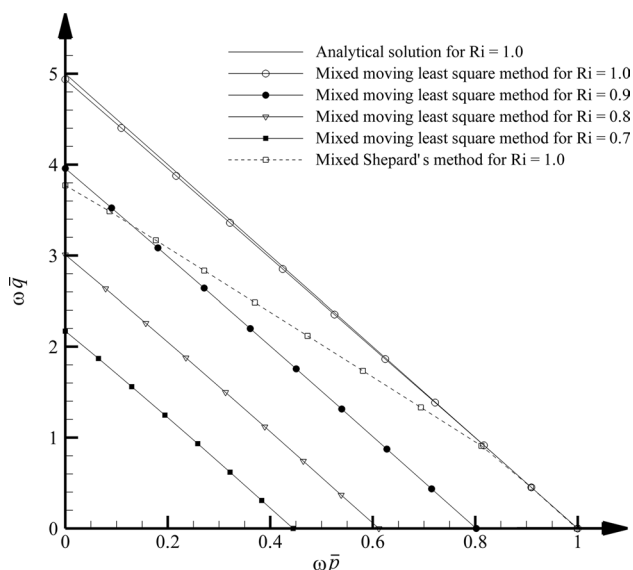


Fig. 3 Bree diagram for the rod obtained for several initial relative densities

$E_0 = 200 \text{ GPa}$, $c_0 = (14 \times 10^{-6}) \text{ }^\circ\text{C}^{-1}$, $Y_0 = 800 \text{ MPa}$, $a = 0.40$, and $b = 0.60$. In this table, ω is the amplification factor for the domain of load variation, $T_{x_{avg}}^r$ represents the average value for the residual stress component in the x direction, and R_{avg} is the average value for the relative density. Additionally, Table 1 shows the amplitudes of variation for T_x^r and R . As can be observed in this table, the MixMLS method presented results very close to the FEM. Additionally, the results from the MixS method presented lower values than those obtained by the MixMLS method and the FEM. In all situations, the MixMLS method presented better results than the MixS method.

The Bree diagram for some values of the initial relative density is shown in Fig. 3. For a dense material ($R_i = 1.0$), a comparison of the MixMLS method with the analytical solution is shown. It can be observed that the numerical solution for the MixMLS method is close to the corresponding analytical solution. For $\bar{p} = 0$, the analytical solution is $\omega\bar{q} = 5$ and the corresponding numerical solution is $\omega\bar{q} = 4.94$; however, both are identical for $\bar{q} = 0$, i.e., $\omega\bar{p} = 1.0$. The numerical results obtained by the mixed Shepard’s method, for a relative density $R_i = 1.0$, showed an increasing difference from the analytical solution for lower values of the axial load.

From Table 1 and Fig. 3, it can be observed that the results obtained by the mixed moving least squares method are close to the corresponding finite element method results. For $R_i = 1.0$, the maximum difference between the analytical solution and the MixMLS method is 1.24%.

To verify the convergence, numerical simulations were performed using 10, 15, and 20 nodal points. For 10 nodes, the method obtained an amplification factor of 2.874, with an error of -1.336 in relation to the analytical solution, i.e., -31.73% . For 15 nodes, the method obtained an amplification factor of 4.178, with an error of -0.03217 , i.e., -0.764% . For 20 nodes, the method obtained an amplification factor of 4.184, with an error of -0.02667 , i.e., -0.633% .

6.2 A square plate of porous material with a central circular hole subjected to a biaxial load

In this section, the shakedown analysis of a square plate made of porous material is presented. The square plate has a width of $2b$ and the central hole has a diameter of $2a$, as shown in Fig. 4. The plate is subjected to a distributed compressive load applied in directions x and y , named p_x and p_y , respectively.

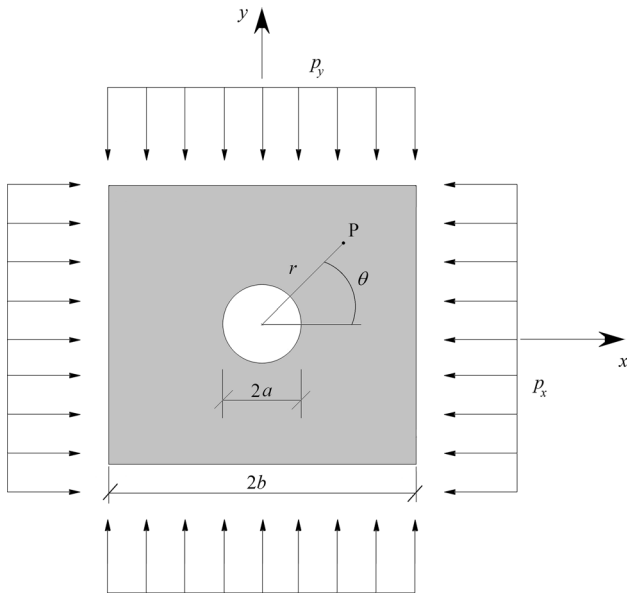


Fig. 4 A square plate subjected to a biaxial load

The loads p_x and p_y can vary independently between prescribed limits:

$$0 \leq p_x \leq \bar{p}_x \quad 0 \leq p_y \leq \bar{p}_y \tag{63}$$

Consequently, the limits for the variation of p_x and p_y define a quadrilateral domain in the load space.

In polar coordinates, the elastic stresses, corresponding to the load p_x , as a function of the angular position θ and the radial distance r from the center of the plate [32] are given by the following expressions:

$$T_r^{ex} = -\frac{p_x}{2} \left(1 - \frac{a^2}{r^2} \right) - \frac{p_x}{2} \left(1 + \frac{3a^4}{r^4} - \frac{4a^2}{r^2} \right) \cos 2\theta \tag{64}$$

$$T_{\theta}^{ex} = -\frac{p_x}{2} \left(1 + \frac{a^2}{r^2} \right) + \frac{p_x}{2} \left(1 + \frac{3a^4}{r^4} \right) \cos 2\theta \tag{65}$$

$$T_{r\theta}^{ex} = \frac{p_x}{2} \left(1 - \frac{3a^4}{r^4} + \frac{2a^2}{r^2} \right) \sin 2\theta \tag{66}$$

The corresponding elastic stresses produced by the load p_y are given by:

$$T_r^{ey} = -\frac{p_y}{2} \left(1 - \frac{a^2}{r^2} \right) + \frac{p_y}{2} \left(1 + \frac{3a^4}{r^4} - \frac{4a^2}{r^2} \right) \cos 2\theta \tag{67}$$

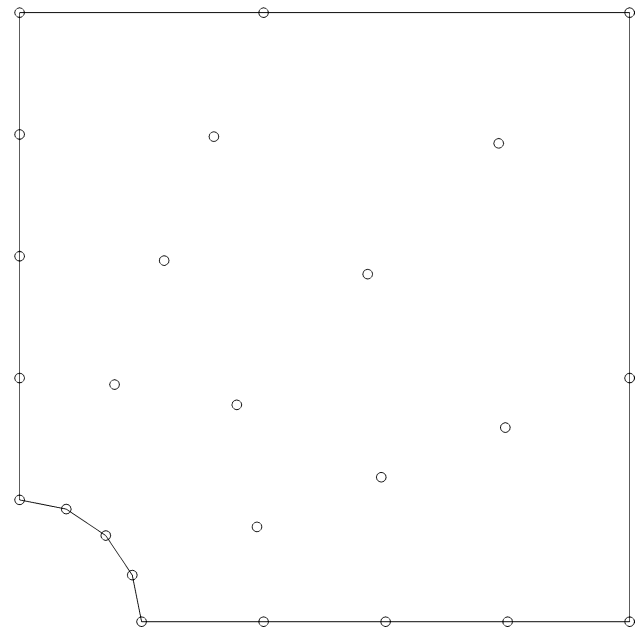


Fig. 5 Distribution of nodes for the shakedown analysis of the plate

$$T_{\theta}^{ey} = -\frac{p_y}{2} \left(1 + \frac{a^2}{r^2} \right) - \frac{p_y}{2} \left(1 + \frac{3a^4}{r^4} \right) \cos 2\theta \tag{68}$$

$$T_{r\theta}^{ey} = -\frac{p_y}{2} \left(1 - \frac{3a^4}{r^4} + \frac{2a^2}{r^2} \right) \sin 2\theta \tag{69}$$

An elastic mapping of the load domain (63) results in a quadrilateral domain in the stress space which is defined by the following components for each vertex:

$$T_r^{e1} = 0 \quad T_{\theta}^{e1} = 0 \quad T_{r\theta}^{e1} = 0 \tag{70}$$

$$T_r^{e2} = T_r^{ex} \quad T_{\theta}^{e2} = T_{\theta}^{ex} \quad T_{r\theta}^{e2} = T_{r\theta}^{ex} \tag{71}$$

$$T_r^{e3} = T_r^{ex} + T_r^{ey} \quad T_{\theta}^{e3} = T_{\theta}^{ex} + T_{\theta}^{ey} \tag{72}$$

$$T_{r\theta}^{e3} = T_{r\theta}^{ex} + T_{r\theta}^{ey}$$

$$T_r^{e4} = T_r^{ey} \quad T_{\theta}^{e4} = T_{\theta}^{ey} \quad T_{r\theta}^{e4} = T_{r\theta}^{ey} \tag{73}$$

Figure 5 shows the distribution of nodes for the shakedown analysis of the plate. Due to the symmetry, only one quarter of the plate is modeled for the numerical analysis by the MixMLS and MixS methods.

The numerical simulations were performed using 25 nodes and a support radius (in the radial basis function (28)) proportional to the radial distance from the center of the plate. The side length of the plate is $2b$ where b is five times the radius a of the central hole (Fig. 4).

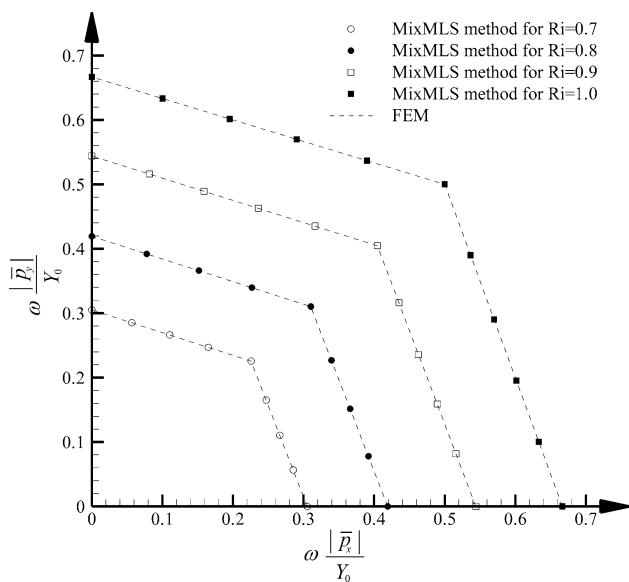


Fig. 6 Bree diagram for a square plate made of porous material with a central circular hole, subjected to a biaxial load, for some initial relative densities

Figure 6 shows the Bree diagram for some values of the initial relative density obtained by the MixMLS method. Additionally, Fig. 6 shows the numerical results obtained by the finite element method [28]. It can be observed that both methods (the MixMLS and FEM) presented similar results for all initial relative densities. The finite element mesh used for the solution of this example has 32 triangular elements, with 81 nodes for velocities and 25 nodes for stresses. The triangular element used in the comparison is a mixed finite element, composed by six nodes of velocities and three nodes of stresses [5, 39].

Table 2 shows the numerical results obtained by the mixed moving least squares, mixed Shepard’s, and finite element method for the particular case of a plate with $b = 100$ mm

and $a = 20$ mm, which is subjected to a biaxial compressive load distribution $\bar{p}_x = \bar{p}_y = 600$ MPa. The plate is made of porous material with a yield limit $Y_0 = 600$ MPa for the base material. The mixed moving least squares method shows similar results to the finite element method [28]; however, the mixed Shepard’s method presents a slight difference with this two methods.

This problem was solved using the exponential radial basis function [3] given by Eq. (27), where the parameter c in the expression is proportional to the radial distance from the center of the plate. Additionally, numerical simulations were performed using 9, 25 and 49 nodes. For 9 nodes, the MixMLS method was unable to obtain a solution; however, for 25 and 49 nodes, the MixMLS method obtained almost the same result for the amplification factor, with a difference of 8.77×10^{-11} .

Figure 7 shows the hydrostatic pressure field, for $R_i = 0.8$, computed through Eq. (8) from the residual stress field obtained by the MixMLS method. Figure 8 shows the relative density field obtained by Eq. (6). It can be observed in Figs. 7 and 8 that the hydrostatic pressure and the relative density are higher around the hole.

6.3 A cantilever beam of porous material

In the following, the shakedown analysis of a cantilever beam made of porous material is presented. The beam has a length b and is subjected to a variable bending moment M and a constant axial compressive load N , as shown in Fig. 9. The cross section of the beam has height h and width t .

The domain for the load variation is presented in Fig. 10. The bending moment M varies between $-\bar{M}$ and \bar{M} , i.e., $-\bar{M} \leq M \leq \bar{M}$, while the compressive axial load \bar{N} is constant.

Figure 11 shows the 35 nodal points used for the numerical shakedown analysis of the cantilever beam by the MixMLS and mixed Shepard’s methods. The support radius

Table 2 Numerical comparison for the mixed moving least squares, mixed Shepard’s, and finite element method for the plate made of porous material

	R_i	ω	$\omega \frac{\bar{p}_x}{Y_0}$	$\omega \frac{\bar{p}_y}{Y_0}$	R_{min}	R_{max}
MixMLS	0.7	0.225719	0.225719	0.225719	0.700	0.709
MixS	0.7	0.203662	0.203662	0.203662	0.700	0.713
FEM	0.7	0.225620	0.225620	0.225620	0.700	0.709
MixMLS	0.8	0.310318	0.310318	0.310318	0.800	0.808
MixS	0.8	0.282493	0.282493	0.282493	0.800	0.812
FEM	0.8	0.310191	0.310191	0.310191	0.800	0.808
MixMLS	0.9	0.404634	0.404634	0.404634	0.900	0.905
MixS	0.9	0.376677	0.376677	0.376677	0.900	0.908
FEM	0.9	0.404549	0.404549	0.404549	0.900	0.905
MixMLS	1.0	0.499972	0.499972	0.499972	1.000	1.000
MixS	1.0	0.483048	0.483048	0.483048	1.000	1.000
FEM	1.0	0.499996	0.499996	0.499996	1.000	1.000

Fig. 7 Hydrostatic pressure field for $R_i = 0.8$ by the MixMLS method using an exponential radial basis function

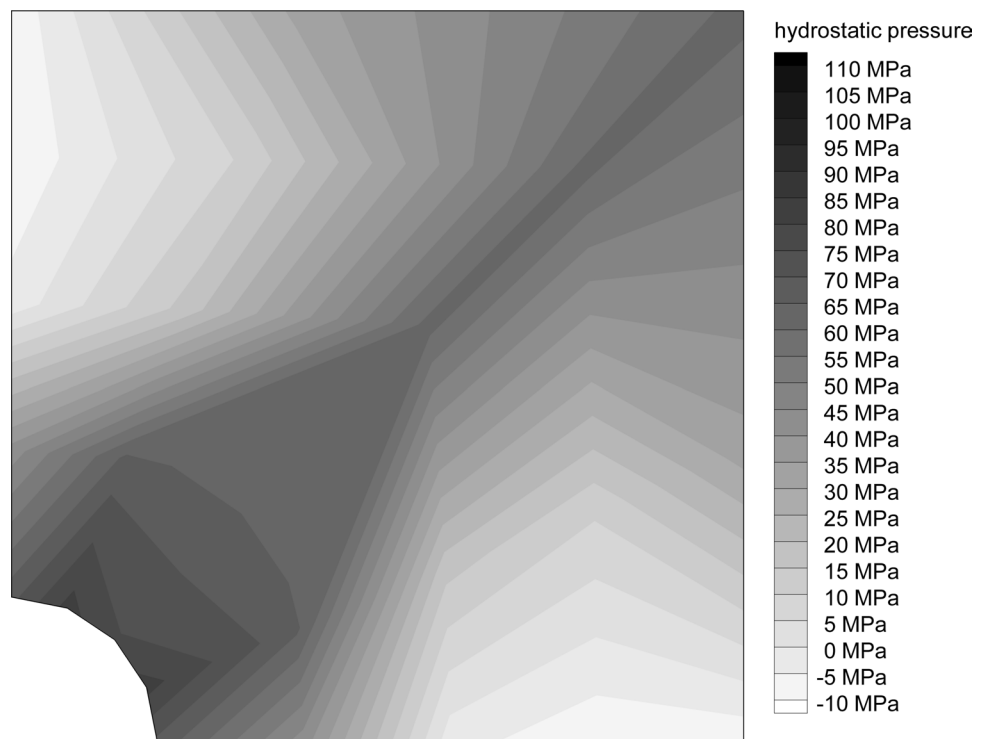
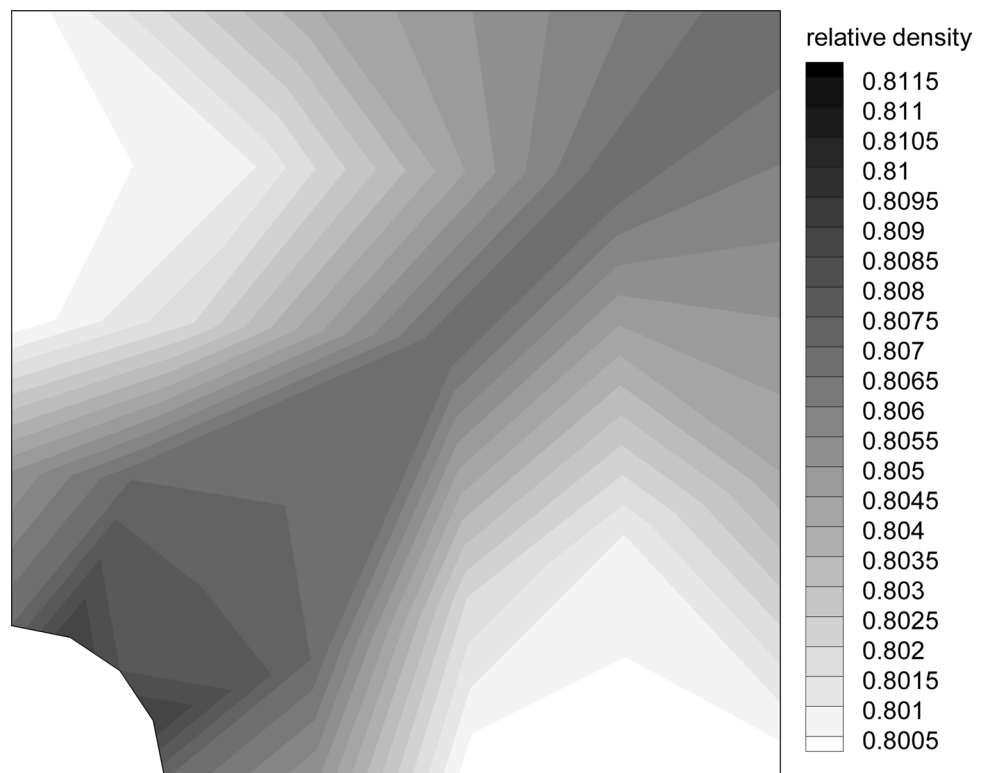


Fig. 8 Relative density field for $R_i = 0.8$ by the MixMLS method using an exponential radial basis function



employed in the radial basis function (28) [34] is equal to 2.1 times the nodal distance in the beam axis direction.

Figure 12 shows the Bree diagram for the MixMLS method for some values of the initial relative density. In

this diagram, N_y and M_y are, respectively, the limit axial load and bending moment for the instantaneous collapse of the beam [36] and are given by:

Fig. 9 Cantilever beam subjected to a bending moment M and an axial load N

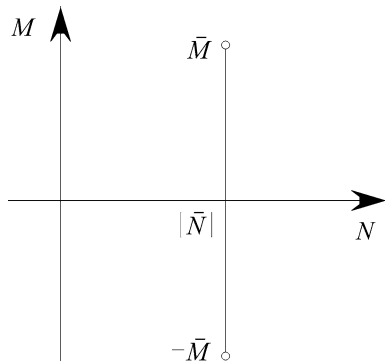
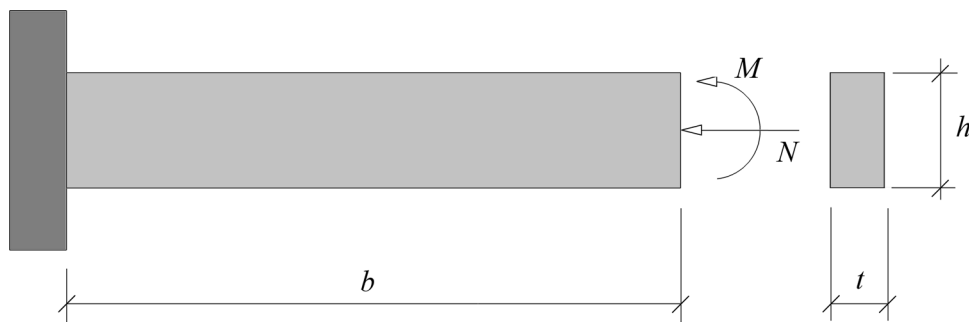


Fig. 10 Load domain for the cantilever beam

$$N_y = t h Y_0 \tag{74}$$

$$M_y = \frac{t h^2 Y_0}{4} \tag{75}$$

As can be observed in Fig. 12, for a relative density equal to 1.0, the numerical solution using the mixed moving least squares method shows a small difference from the analytical solution for low and high axial load values; however, the difference is greater for intermediate loads. The maximum difference between the analytical and the numerical solution by the MixMLS is approximately 6.07%. The mixed Shepard’s method failed to obtain a numerical solution for the cantilever beam problem.

For the particular case of a beam with a length $b = 10$ m, height $h = 1$ m, thickness $t = 0.10$ m, and yield limit for the

base material $Y_0 = 800$ MPa, subjected to a variable bending moment within the limits -300 kN m and 300 kN m, i.e., $\bar{M} = 300$ kN m, and a constant compressive axial load $\bar{N} = 3$ MN, the numerical amplification factor ω obtained by the mixed moving least squares method is 19.93 and the analytical solution for this case is 20.51 [36], with a difference of -0.583 . To verify the convergence, numerical simulations were performed using 14, 21, 28, and 35 nodal points. For 14 nodes, the MixMLS method was unable to obtain a solution. For 21, 28, and 35 nodes, the method obtained 19.46, 19.42, and 19.93, respectively, for the amplification factor, with the following percentage error: -5.11% , -5.33% , and -2.84% , respectively.

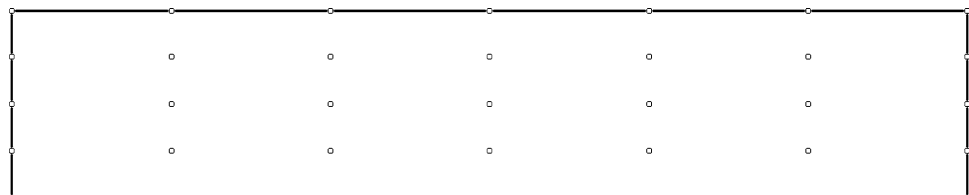
7 Conclusion

In this paper, two meshless methods were presented for the numerical solution of the shakedown analysis of porous material, namely the mixed moving least squares (MixMLS) method and the mixed Shepard’s (MixS) method.

In the presented examples, the MixMLS method showed good results when compared with analytical solutions and previously published results obtained by the finite element method; however, the results obtained by the mixed Shepard’s method were less precise than the results obtained by the corresponding MixMLS method and for one example, the mixed Shepard’s method failed to obtain the numerical solution.

As expected, in all the performed numerical simulations, as the initial relative density approaches the unity, the porous material behavior approaches the behavior of the dense material.

Fig. 11 Node distribution for the MixMLS and mixed Shepard’s methods



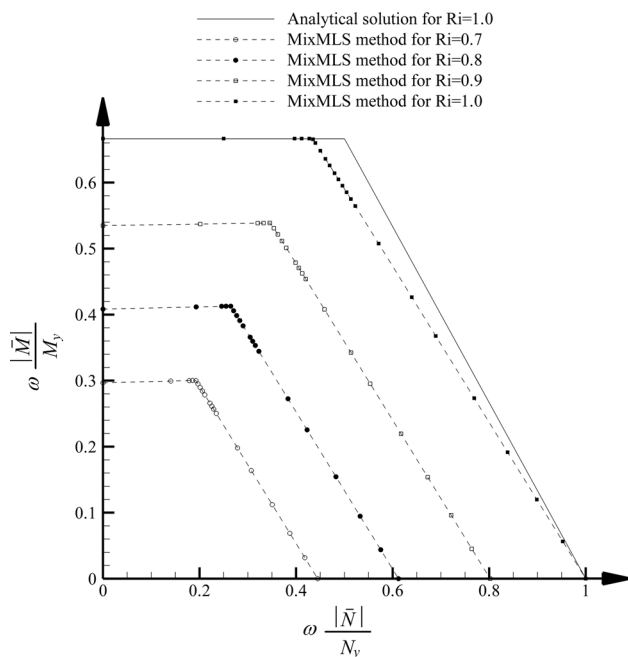


Fig. 12 Bree diagram for a cantilever beam made of porous material by the mixed moving least squares method, for some initial relative densities

Despite the higher computational cost, the implementation of the MixMLS method is easier than the other traditional numerical methods.

Acknowledgements This work was partially supported by the Coordenação de Aperfeiçoamento de Pessoal de Nível Superior-Brasil (CAPES), Finance Code 001.

References

- Alves LMM, Martins PAF, Rodrigues JMC (2006) A new yield function for porous materials. *J Mater Process Technol* 179:36–43
- Belytschko T (1972) Plane stress shakedown analysis by finite elements. *Int J Mech Sci* 14:619–625
- Belytschko T, Lu YY, Gu L (1994) Element-free Galerkin methods. *Int J Numer Methods Eng* 37:229–256
- Belytschko T, Krongauz Y, Organ D, Fleming M, Krysl P (1996) Meshless methods: an overview and recent developments. *Comput Methods Appl Mech Eng* 139:3–47
- Borges L, Zouain N, Huespe AE (1996) A nonlinear optimization procedure for limit analysis. *Eur J Mech A/Solids* 15:487–512
- Chen HF, Ponter ARS (2001) Shakedown and limit analyses for 3-D structures using the linear matching method. *Int J Press Vessels Pip* 78(6):443–451
- Chen S, Liu Y, Li J, Cen Z (2011) Performance of the MLPG method for static shakedown analysis for bounded kinematic hardening structures. *Eur J Mech A/Solids* 30:183–194
- Doraivelu SM, Gegel HL, Gunasekera JS, Malas JC, Morgan JT (1984) A new yield function for compressible P/M materials. *Int J Mech Sci* 26(9):527–535
- El Ghezal MI, Doghri I (2018) Porous plasticity: predictive second moment homogenization models coupled with Gurson's single cavity stress–strain solution. *Int J Plast* 108:201–221
- Fonseca AR (2011) Algoritmos eficientes em métodos sem malha. Tese de D.Sc., Universidade Federal de Minas Gerais, Belo Horizonte Minas Gerais Brasil
- Garcea G, Leonetti L (2011) A unified mathematical programming formulation of strain driven and interior point algorithms for shakedown and limit analysis. *Int J Numer Methods Eng* 88:1085–1111
- Green RJ (1972) A plasticity theory for porous solids. *Int J Mech Sci* 14:215–224
- Guedes CMCFM (2006) Método sem malha em problemas de mecânica computacional. Aplicação a processos de enformação plástica. Tese de D.Sc., Faculdade de Engenharia do Porto, Porto Portugal
- Gurson AL (1977) Continuum theory of ductile rupture by void nucleation and growth: part I. Yield criteria and flow rules for porous ductile media. *J Eng Mater Technol* 76:2–15
- Heckel RW (1961) Density–pressure relationships in powder compaction. *Trans Metall Soc AIME* 221:671–675
- Koiter W (1960) Progress in solid mechanics, vol 1, 1st edn. North-Holland Publ. Co., Amsterdam, pp 167–221 (Chap IV: General theorems for elastic–plastic structures)
- Krabbenhøft K, Lyamin A, Sloan S (2007) Formulation and solution of some plasticity problems as conic programs. *Int J Solids Struct* 44:1533–1549
- Lewis RW, Khoei AR (2001) A plastic model for metal powder forming processes. *Int J Plast* 17:1659–1692
- Maier G (1968) A quadratic programming approach for certain classes of non linear structural problems. *Meccanica* 3(2):121–130
- Maier G (1969) Shakedown theory in perfect elastoplasticity with associated and nonassociated flow-laws: a finite element, linear programming approach. *Meccanica* 4(3):250–260
- Makrodimopoulos A (2006) Computational formulation of shakedown analysis as conic quadratic optimization problem. *Mech Res Commun* 33:72–83
- Melan E (1938) Zur Plastizität des räumlichen Kontinuums. *Ing Arch* 8:116–126
- Nguyen AD, Hachemi A, Weichert D (2008) Application of the interior-point method to shakedown analysis of pavements. *Int J Numer Methods Eng* 44:414–439
- Park JJ (1995) Constitutive relations to predict plastic deformations of porous metals in compaction. *Int J Mech Sci* 37(7):709–719
- Peng H, Liu Y, Chen H, Shen J (2018) Shakedown analysis of engineering structures under multiple variable mechanical and thermal loads using the stress compensation method. *Int J Mech Sci* 140:361–375
- Peng H, Liu Y, Chen H (2019) A numerical formulation and algorithm for limit and shakedown analysis of large-scale elastoplastic structures. *Comput Mech* 63(1):1–2
- Ruiz CCLP, Silveira JL (2015) Mixed moving least-squares method for shakedown analysis. *Arch Appl Mech* 85(6):775–791
- Ruiz CCLP, Silveira JL (2018) Shakedown analysis for porous materials. *Eur J Mech A/Solids* 69:124–134
- Shepard D (1968) A two-dimensional interpolation function for irregularly-spaced data. In: ACM national conference, pp 517–524
- Shima S, Oyane M (1975) Plasticity theory for porous metals. *Int J Mech Sci* 18:285–291
- Silveira JL, Zouain N (1997) On extremum principles and algorithms for shakedown analysis. *Eur J Mech A/Solids* 16(5):757–778
- Timoshenko SP, Goodier JN (1987) Theory of elasticity, 3rd edn. McGraw-Hill, New York

33. Weichert D, Ponter A (2014) A historical view on shakedown theory. In: Stein E (ed) *The history of theoretical, material and computational mechanics: mathematics meets mechanics and engineering*. Lecture notes in applied mathematics and mechanics, vol 1. Springer, Berlin, pp 169–193
34. Wu Z (1995) Compactly supported positive definite radial functions. *Adv Comput Math* 4:283–292
35. Zhang J, Shen WQ, Oueslati A, De Saxcé G (2017) Shakedown of porous materials. *Int J Plast* 95(Supplement C):123–141
36. Zouain N, Silveira JL (1999) Extremum principles for bounds to shakedown loads. *Eur J Mech A/Solids* 18:879–901
37. Zouain N, Silveira JL (2000) Variational principles for shakedown analysis. In: Weichert D, Maier G (eds) *Inelastic analysis of structures under variable loads theory and engineering applications*. Kluwer Academic Publishers, Dordrecht, pp 147–165
38. Zouain N, Borges L, Silveira JL (2002) An algorithm for shakedown analysis with nonlinear yield functions. *Comput Methods Appl Mech Eng* 191:2463–2481
39. Zouain N, Borges L, Silveira JL (2014) Quadratic velocity-linear stress interpolations in limit analysis. *Comput Methods Appl Mech Eng* 98:469–491

Publisher's Note Springer Nature remains neutral with regard to jurisdictional claims in published maps and institutional affiliations.